IET Microwaves, Antennas & Propagation

Research Article

IET Journals
The Institution of Engineering and Technology

Wireless resonant energy link for pulse generators implanted in the chest

ISSN 1751-8725
Received on 23rd March 2017
Revised 16th August 2017
Accepted on 1st September 2017
E-First on 27th October 2017
doi: 10.1049/iet-map.2017.0250
www.ietdl.org

Giuseppina Monti[1] ✉, *Maria V. De Paolis*[1], *Laura Corchia*[1], *Luciano Tarricone*[1]

[1]*Department of Engineering for Innovation, University of Salento, via per Monteroni, Lecce, Italy*

✉ *E-mail: giuseppina.monti@unisalento.it*

Abstract: This study investigates the feasibility of using the MedRadio band for wirelessly transmitting power to a rechargeable medical device implanted in the chest. In particular, a wireless energy link operating at 403 MHz and based on an inductive coupling between two planar resonators is considered, and its performance is assessed through simulations and experimental tests. Results show that a maximum value of the measured power transfer efficiency of ~23% is achieved. Furthermore, the possibility of using the link for recharging a lithium-ion battery of a pulse generator implanted in the chest at a depth of 5 mm is discussed, and the compliance with safety regulations is verified. Reported results demonstrate that the proposed link can be used to charge a lithium-ion battery with a capacity up to 7.2 mAh, while inducing a peak of the specific absorption rate averaged over 1 g of tissue <1.6 W/kg.

1 Introduction

Implantable medical devices (IMDs) are essential for treating several diseases such as heart failures, acute forms of diabetes, chronic pain etc. In particular, implantable neurostimulators are commonly adopted to relieve the symptoms associated with neurological disorders. This procedure is called deep brain stimulation (DBS), and it has been approved by the US Food and Drug Administration for the treatment of Parkinson's disease, essential tremor, and dystonia [1].

A typical DBS system consists of four main components: the leads, the electrodes, the extensions, and the neurostimulator (i.e. the implanted pulse generator – IPG). The electrodes are implanted in specific areas of the brain and are connected via leads to the IPG; this, in turn, is located near the collarbone or in a lateral chest wall. The IPGs used in DBS are similar to cardiac pacemakers and deliver balanced biphasic pulse. Common IPGs work on battery; hence, they have a limited lifetime (usually in the order of 2–5 years [2]) and have to be periodically replaced through surgery.

Recently, some IPGs equipped with wirelessly rechargeable batteries have been proposed [3, 4]; these IPGs resort to wireless power transmission (WPT) for achieving a longer lifetime (up to 10–20 years).

WPT is the process of wirelessly transmitting power from a transmitting to a receiving device. Depending on the requirements of the specific application, WPT can be implemented by using either antennas (far-field WPT links) or inductively/capacitively coupled devices (near-field links) [5–7].

With regard to medical devices, considering that they are often implanted a few centimetres under the skin and because of the electrical and magnetic characteristics of the biological tissues, the use of a near-field link based on inductive coupling is currently the most widespread solution.

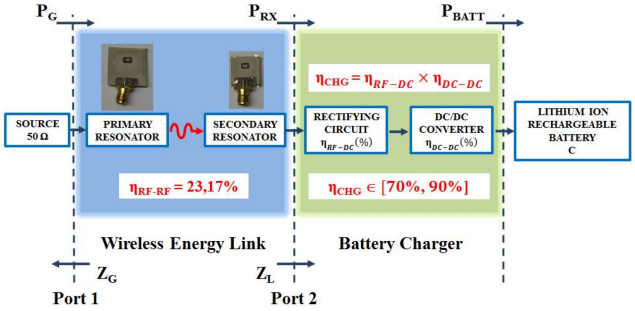

Fig. 1 *Schematic representation of a wireless battery charger*

Additionally, a crucial role is also played by the operating frequency. In fact, electromagnetic (EM) energy absorption in human tissues increases as the frequency increases. Accordingly, most of the WPT links for IMD proposed so far in the literature operate at very low frequencies, not reserved to medical devices [8–12].

Although this choice allows to minimise the EM energy absorption in human tissues and, as a consequence, to maximise the power transfer efficiency of the link, it imposes the use of different devices, eventually integrated in the same apparatus, for power and data transmission [10].

In this regard, the solution proposed in [13] of operating in the MedRadio (Medical Device Radiocommunications Service) core band reserved to medical devices [14] appears as a valid and attractive alternative.

Accordingly, in our previous works [15, 16], we presented a WPT link operating at 403 MHz and potentially suitable to be used for both data and power transmission between an IPG implanted in the chest and an external controller. In more detail, the link proposed in [15] adopts a resonant scheme (i.e. the transmitter and the receiver are designed so to resonate at the same frequency), thus resulting in a so-called wireless resonant energy link (WREL). In fact, as widely demonstrated in the literature [17–19], the use of a resonant inductive coupling instead of an inductive coupling allows improving the efficiency of the link.

Assuming that the wireless link has to connect a generator with impedance R_G to a load R_L, see Fig. 1, in this paper, the following definition is adopted for the RF-to-RF power transfer efficiency (η_{RF-RF}):

$$\eta_{RF-RF} = \frac{\text{Power delivered to the load } R_L}{\text{Available power from the source}} = \frac{P_{RX}}{P_G} = |S_{21}|^2 \quad (1)$$

where S_{21} is the transmission coefficient of the generalised scattering matrix of the link [20] calculated by using R_G as normalisation impedance at port 1 and R_L as normalisation impedance at port 2 (Fig. 1).

According to this choice of the normalisation impedances, the parameter S_{21} takes into account the power reflected at port 1 towards the generator when the generator has an input impedance

R_G and the power reflected at port 2 towards the network when the load is R_L.

The quantity expressed in (1) coincides with the transducer gain of a two-port network as defined in [20]; it can be easily seen that for given values of the power available from the source, maximising η_{RF-RF} is equivalent to maximise the power delivered to the load. It is worth observing that the expression of η_{RF-RF} given in (1) is different from the one adopted in [15]; however, this definition is the one commonly used in the context of WPT [21] and allows simplifying the comparison with previously published results.

According to (1), the WPT link presented in [15] has a measured power transfer efficiency of 15.27%. With respect to [15], further results and discussions are reported in this paper. In particular, an improved version of the link having a power transfer efficiency of 23.17% is presented.

With regard to the use of WPT for medical implants, a comparison of the link proposed in this paper with previously published works is reported in Table 1.

As expected, the proposed link has an efficiency higher than the one obtained for links operating at higher frequencies (see [22, 23]). Similarly, it can be seen that, with respect to WPT links operating at lower frequencies (see [8–11]), the one presented herein is characterised by lower values of the power transfer efficiency. These data confirm the advantages of using an operating frequency in the range that goes from some hundreds of kilohertz to some megahertz in order to maximise η_{RF-RF}.

However, for medical devices implanted at few millimetres under the skin, the results reported in this paper demonstrate that the value that has been obtained for η_{RF-RF} allows the recharging of a lithium-ion battery having a capacity up to 7.2 mAh with a reasonable recharging time (6 h), thus validating the possibility of using the MedRadio band for recharging medical implants.

The paper is organised as follows. The proposed wireless energy link is presented in Section 2, a sensitivity analysis is described in Section 3, and experimental data are given in Section 4. The feasibility of using the WREL for recharging an IPG for DBS in compliance with safety regulations is discussed in Section 5, and some conclusions are drawn in Section 6.

2 Resonator geometry and numerical results

The proposed WPT link exploits a magnetic coupling between two planar resonators on an Arlon DiClad 880 substrate ($\varepsilon_r = 2.17$, $\tan\delta = 0.0009$) with a thickness of 0.508 mm (Fig. 2*a*).

Each resonator consists of a distributed inductance (a planar loop) loaded by a lumped capacitor. The configuration of the link is the same considered in [15], and it is illustrated in Fig. 2*a*: it is assumed that the transmitting resonator (primary resonator) operates in direct contact with the skin and that the receiving resonator (secondary resonator) is implanted in the muscle below a layer of skin and fat. In more detail, the resonators were optimised by assuming that the layers of skin and fat have a thickness of 2 mm (d_{skin} and d_{fat}) and that the secondary resonator is implanted in the muscle layer at a depth of 1 mm (i.e. dt = 1 mm), thus resulting in an overall distance between the two resonators of 5 mm (d) (Fig. 2*a*).

Table 2 summarises the values assumed for the EM parameters of human tissues; the IT'IS Foundation database [24] was taken as a reference.

The starting point of the design process of the resonators was the geometry presented in [15]. In particular, taking into account results reported in [15], the set-up adopted for both full-wave simulations (accuracy, mesh properties etc.) and measurements was optimised in order to reduce the mismatch between numerical and experimental data.

According to the results obtained by full-wave simulations performed by using the optimised set-up, the resonators presented in [15] were finely optimised in order to improve the power transfer efficiency at 403 MHz (i.e. at the central frequency of the MedRadio band).

In more detail, referring to Figs. 2*b* and *c*, the geometry of the planar loops adopted for implementing the distributed inductance of the resonators was optimised in order to maximise the magnetic coupling between the primary and the secondary resonators while the values of the lumped capacitors were used to tune the frequency of resonance at 403 MHz.

The parameters of the planar loops that were optimised are: radius of the inner loops and number of turns; the width of the strips of copper; and the gap between different turns. Optimisations were performed by using 50 Ω microwave ports (discrete ports) placed as shown in Figs. 2*b* and *c*, the goal was to maximise the $|S_{21}|$ parameter, which is directly related to the definition adopted in this paper for the power transfer efficiency of the link, while keeping the dimensions of the loops as small as possible.

Table 1 Performance of WPT links for medical devices

Ref.	Operating frequency	Geometry of the receiver	Technology	Dimensions of the receiver	Efficiency (%)/gain	Implantation depth, mm
[8]	1 MHz/5 MHz	printed spiral coil	inductive WPT	20 mm (diameter)	41.2% at 1 MHz, 85.8% at 5 MHz	10
[9]	300 kHz/13.56 MHz	coil	magnetic resonant coupling	17.65 mm (radius)	78% at 300 kHz, 89% at 13.56 MHz	10
[10]	6.78 MHz (WPT link), 402–405 MHzMICS band (data link)	resonant spiral coil, loop loaded with a magnetic core	resonant inductive link	<(10 × 10) mm^2, (14 × 14) mm^2	35%−27 dBi (simulated)	20
[11]	10 MHz	coil	inductive coupling	250 mm^2	82% at 10 MHz (simulated)	5
[12]	13.56 MHz	printed spiral coil	inductive WPT	(10 × 10) mm^2	15.2% at 8 MHz (simulated)	10
[22]	1.5 GHz (WPT link)400 MHz (data link)	solenoid, spiralled patch PIFA antenna	midfield energy transfer	9 mm (diameter) 20 mm (length), (20.5 × 30) mm^2	0.59% at 1.5 GHz−32 dBi	45
[23]	1.7 GHz	coil	midfield energy transfer	1 mm (diameter)	0.045% at 1.7 GHz	50
[13]	401–406 MHz (MedRadio band)	square split ring resonator	resonant inductive coupling	(9.5 × 9.5) mm^2	5.24% at 403 MHz	5
[15, 16]	401–406 MHz (MedRadio band)	planar loaded by a lumped capacitor	resonant inductive coupling	(10.14 × 10.14) mm^2	15.27% at 403 MHz	5
this work	401–406 MHz (MedRadio band)	planar loaded by a lumped capacitor	resonant inductive coupling	(9.87 × 9.87) mm^2	23.17% at 403 MHz	5

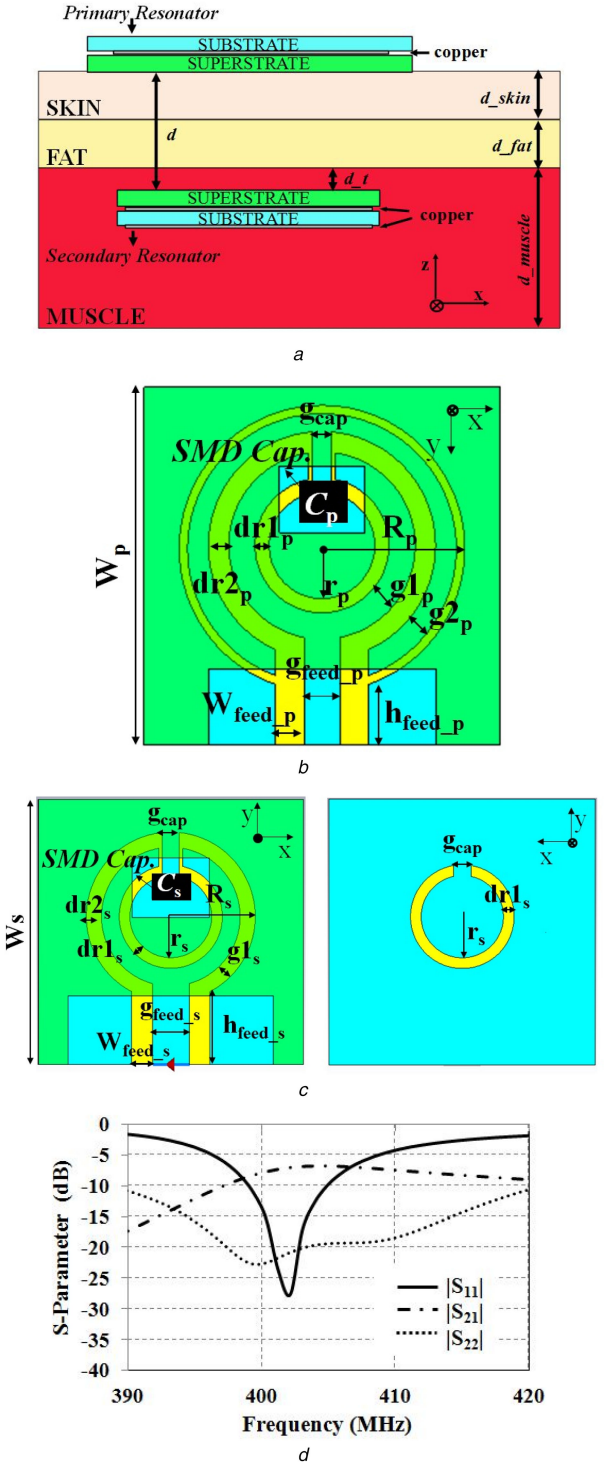

Fig. 2 *Configuration of the WPT link and geometry of the resonators proposed in this paper*

(a) Configuration of the wireless resonant inductive link adopted in full-wave simulations: $d = 5$ mm, $dt = 1$ mm, $d_{skin} = 2$ mm, $d_{fat} = 2$ mm, $d_{muscle} = 16$ mm, ***(b)*** Geometry of the primary resonator, ***(c)*** Front and back view of the secondary resonator, ***(d)*** Generalised scattering parameters of the proposed inductive link calculated by means of full-wave simulations

Table 2 Parameters adopted in full-wave simulations for human tissues

403 MHz	Skin	Fat	Muscle
ε_r	46.7	11.6	57.1
σ, S/m	0.68	0.081	0.797
ρ, kg/m^3	1090	1109	911

The final geometries guaranteeing the best results are illustrated in Figs. 2*b* and *c*; the corresponding parameters are summarised in Table 3 (see Figs. 2*b* and *c* for the description of each parameter).

The link described in [15] used two resonators, the primary and the secondary resonators, with the same geometry. On the other hand, the link here presented adopts a different geometry for the primary and the secondary resonator; in particular, the secondary resonator has the same geometry described in [15] with optimised dimensions. As for the primary resonator, the solution presented in this work is a single-side design consisting of three concentric loops.

As in [15], for both the primary and the secondary resonator, an Arlon AR1000 superstrate ($\varepsilon_r = 9.7$, and tan $\delta = 0.003$, thickness = 0.610 mm) was used to improve the magnetic coupling.

The primary resonator occupies an area of ~16.24 mm × 16.24 mm over a substrate of dimensions 20.48 mm × 20.48 mm, while the secondary resonator occupies an area of 9.86 mm × 9.86 mm over a substrate of dimensions 15.48 mm × 15.48 mm. The thickness of the resonators is equal to 1.15 and 1.18 mm for the primary and the secondary resonator, respectively.

Fig. 2*d* shows the numerical data obtained for the generalised scattering parameters normalised at both ports with respect to a 50 Ω impedance. The values calculated at 403 MHz are: $|S_{11}| = -17.10$ dB, $|S_{21}| = -6.83$ dB, and $|S_{22}| = -20.04$ dB. According to the definition given in (1), from numerical data, the RF-to-RF power transfer efficiency of the link when $R_G = R_L = 50\ \Omega$ is equal to 20.75% at 403 MHz.

3 Sensitivity analysis

According to the description reported in Section 2, the proposed link was optimised for operating with the secondary resonator implanted in a layer of muscle and below a layer of skin and fat (Fig. 2*a*). In more detail, the dimensions of the resonators were optimised by assuming an overall distance between the two resonators of 5 mm (*d*), an implantation depth into the muscle layer of 1 mm (i.e. d*t* = 1 mm), and a value of 2 mm for both the layer of skin (d_{skin}) and fat (d_{fat}).

However, the thicknesses of the human tissues may vary significantly among different people; therefore, a key point is to evaluate the dependence of the performance of the link on these parameters. Accordingly, simulations were performed by varying the thickness of the skin layer (d_{skin}) and the one of the fat layer (d_{fat}); the case of a deeper implantation depth inside the muscle layer (d*t*) has been also considered. As per problems related to misalignments, both lateral misalignments in the *xy* plane and misalignments due to small rotations of the implanted resonator are possible. The case of lateral misalignments can be easily solved by adjusting the position of the external resonator; while the case of a rotation is more difficult to correct by acting on the position of the external resonator and has been investigated through full-wave simulations.

Finally, the case of the primary resonators not in direct contact with the skin has also been considered.

3.1 Sweep of the thickness of the skin layer

Referring to Fig. 2*a*, the performance of the link was investigated by varying the thickness of the skin layer (d_{skin}) in the range of (2–3) mm, while keeping constant the thickness of the fat layer (i.e. $d_{fat} = 2$ mm) and the implantation depth into the layer of muscle (i.e. d*t* = 1 mm). The range of (2–3) mm for the variability of the thickness of the skin layer was derived by Clarys and Marfell-Jones [25].

It is worth observing that increasing the value of the thickness of the skin layer corresponds to increase the distance between the two resonators.

Fig. 3*a* shows the effect of the variation of the skin thickness on the efficiency of the proposed link. In more detail, the results obtained by using the $|S_{21}|$ parameter normalised at both ports with respect to an impedance of 50 Ω are reported.

Table 3 Dimensions of the resonators

Primary resonator		Secondary resonator	
Symbol	Value	Symbol	Value
C_p[a]	18 pF	C_s	18 pF
$dr1_p$	0.82 mm	$dr1_s$	0.62 mm
$dr2_p$	1.17 mm	$dr2_s$	0.88 mm
$g1_p$	1.51 mm	$g1_s$	1.04 mm
$g2_p$	1.11 mm	g_{cap}	1.01 mm
g_{cap}	1.01 mm	g_{feed_s}	2.15 mm
g_{feed_p}	2.07 mm	h_{feed_s}	4.26 mm
h_{feed_p}	5.41 mm	r_s	2.39 mm
r_p	3.03 mm	R_s	4.93 mm
R_p	8.12 mm	W_{feed_s}	1.20 mm
W_{feed_p}	1.50 mm	W_s[a]	15.48 mm
W_p	20.48 mm		

[a]Subscript letter p or s denotes the primary and the secondary resonators, respectively.

As expected, a reduction in the efficiency can be observed. This effect seems to be mainly due to the increase in the distance between the resonators. However, at the frequency of interest (i.e. 403 MHz), the RF-to-RF power transfer efficiency is always >13.21%.

3.2 Sweep of the thickness of the fat layer

As for the dependence of the performance of the proposed link on the thickness of the fat layer, full-wave simulations were performed by varying d_{fat} in the range of (2–7) mm [26], while keeping constant the thickness of the skin layer (i.e. $d_{skin} = 2$ mm) and of the implantation depth inside the muscle layer (i.e. $dt = 1$ mm).

It is worth noticing that, similarly to the case of the sweep of the thickness of the skin layer, also in this case increasing the thickness of the fat layer corresponds to increase the distance between the resonators (d).

The efficiency calculated for different values of d_{fat} is given in Fig. 4*a*. As expected, a reduction in η_{RF-RF} can be observed.

A comparison of Figs. 3*a* and 4*a* suggests that the reduction in the transfer efficiency is mainly due to the increase in the distance between the resonators. In fact, it can be seen that the values of η_{RF-RF} corresponding to the distance (d) of 6 mm are very close to each other for both sweeps.

3.3 Sweep of the implantation depth into the muscle layer

In this section, the implantation depth into the muscle layer (dt) was investigated. With reference to Fig. 2*a*, full-wave simulations were performed by varying dt in the range (1–4) mm, thus corresponding to a distance (d) between the two resonators in the range (5–8) mm.

A comparison of the results obtained for the parametric sweeps reported in Figs. 4*a* and 5*a* confirms that the degradation of the performance of the link is mainly due to the increase in the distance between the resonators.

In fact, although results reported in Figs. 4*a* and 5*a* concern the variation of the thickness of two biological layers having very different dielectric parameters, the efficiency calculated for a given value of d is almost the same for both sweeps.

3.4 Effect on the performance of small rotations of the implanted resonator

In order to investigate the effect on the performance of possible rotations of the implanted resonator, the case illustrated in Fig. 6 and related to rotations in the yz plane has been analysed. According to the suggestions received by surgeons, very small rotations of the medical implant can occur due to movements of the implant bearer. Accordingly, a rotation angle in the range of (0°, 7°) has been considered.

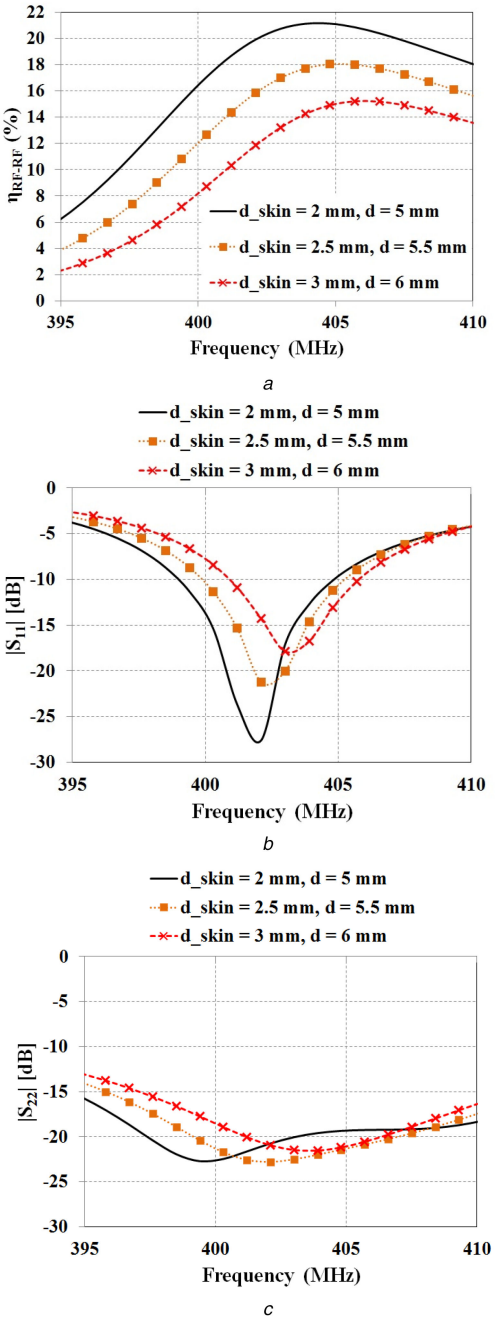

Fig. 3 *Parametric sweep of the thickness of the skin layer*
(a) Effect of the variation of skin thickness (d_{skin}) on the RF-to-RF power transfer efficiency of the proposed WPT link. The solid black line denotes the η_{RF-RF} obtained for the initial configuration depicted in Fig. 2*a* (i.e. for $d_{skin} = 2$ mm, $d_{fat} = 2$ mm, $dt = 1$ mm, and $d = 5$ mm), ***(b)*** Effect of skin thickness (d_{skin}) on the $|S_{11}|$ parameter, ***(c)*** Effect of skin thickness (d_{skin}) on the $|S_{22}|$ parameter

The results achieved by full-wave simulations for the efficiency are summarised in Fig. 6; as it can be seen, small rotations of the implanted resonator in the yz plane do not compromise the performance.

3.5 Primary resonator not in direct contact with the skin

Finally, the performance of the link has been evaluated in the case where the primary resonator is not in direct contact with the skin.

This analysis is of interest because, in order to make comfortable the recharge process and to keep the external resonator in the right position during the recharge process, a possible solution could be to embed the primary resonator into an elastic wearable band. Accordingly, full-wave simulations have been performed by

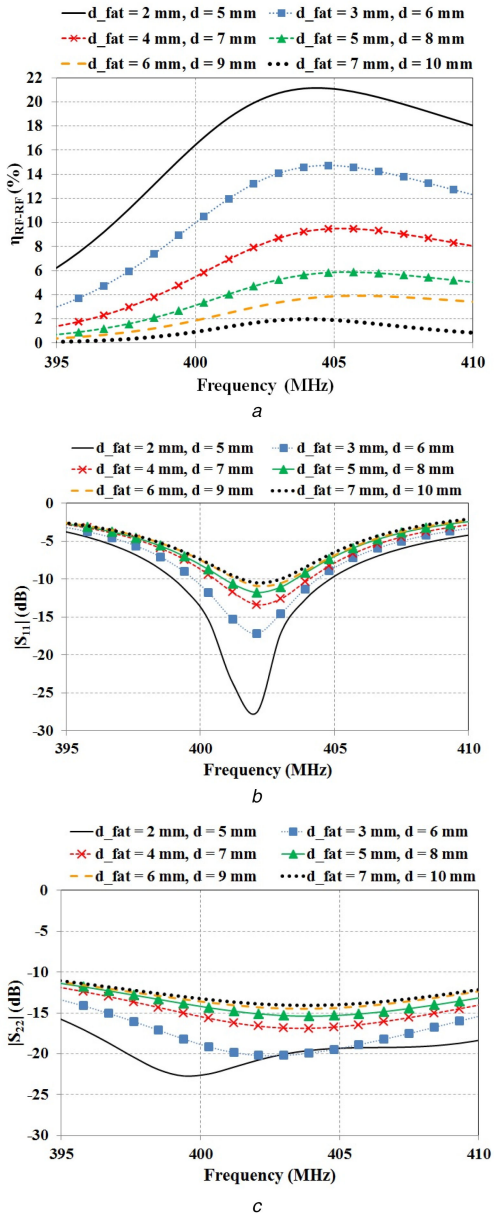

Fig. 4 *Parametric sweep of the thickness of the fat layer*
(a) RF-to-RF power transfer efficiency of the proposed WPT link calculated by full-wave simulations for different values of d_{fat}. The solid black line denotes the η_{RF-RF} obtained for the initial configuration depicted in Fig. 2*a* (i.e. for $d_{skin} = 2$ mm, $d_{fat} = 2$ mm, $dt = 1$ mm, and $d = 5$ mm), ***(b)*** Effect of the thickness of the fat layer on the $|S_{11}|$ parameter, ***(c)*** Effect of the thickness of the fat layer on the $|S_{22}|$ parameter

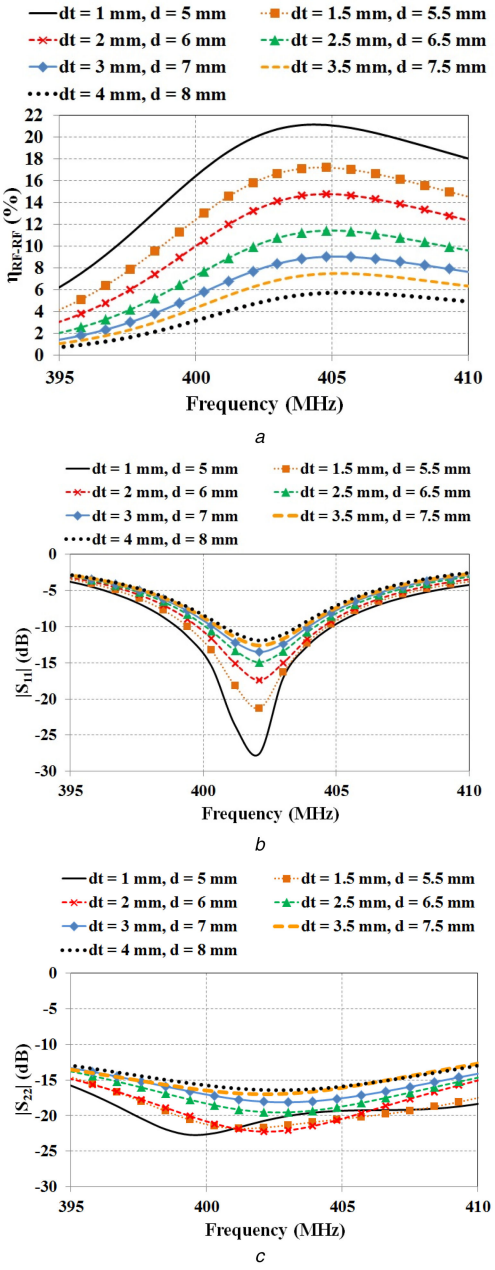

Fig. 5 *Parametric sweep of the implantation depth into the muscle layer*
(a) RF-to-RF power transfer efficiency of the proposed WPT link for different values of the implantation depth into the muscle layer. The solid black line denotes the η_{RF-RF} obtained for the initial configuration depicted in Fig. 2*a* (i.e. for $d_{skin} = 2$ mm, $d_{fat} = 2$ mm, $dt = 1$ mm, and $d = 5$ mm), ***(b)*** Effect of the implantation depth into the muscle layer on the $|S_{11}|$ parameter, ***(c)*** Effect of the implantation depth into the muscle layer on the $|S_{22}|$ parameter

placing the primary resonator at a distance d_{pr} from the skin, being d_{pr} the thickness of a textile material with a relative electric permittivity ε_{tex}. The cases of d_{pr} equal to 1 and 2 mm and ε_{tex} equal to 1 and 1.5 have been considered. In fact, most of the textile materials that could be of interest for realising the wearable band (e.g. cotton, polar fleece, jeans etc.) have a relative permittivity in the range (1–1.6); as per the thickness, a reasonable value seems to be in the range (1–2) mm. The achieved results are given in Figs. 7*a–c*; the results corresponding to the nominal configuration (i.e. for $d_{pr} = 0$) are also reported for comparison.

From Fig. 7*a*, it can be seen that the level of matching and the frequency of resonance of the primary resonator depends on d_{pr} and this leads to a dependence of the efficiency of the link on d_{pr} (Fig. 7*c*). However, from Fig. 7*d*, where the results obtained by tuning the loading capacitor of the primary resonator are reported, it can be seen that the performance degradation due to values of d_{pr} different from zero can be solved by using a variable capacitor as loading capacitor of the primary resonator.

4 Experimental results

A prototype of both resonators was fabricated by using the LPKF ProMat S103 circuit board micro-cutter. Photographs are given in Figs. 8*a* and *b* and the set-up adopted for measurements is illustrated in Figs. 8*c* and *d*.

Minced pork was used in order to mimic the presence of human tissues. In fact, in the MedRadio band, minced pork provides a good approximation for the characterisation of wireless devices implanted in the chest [13, 27].

Two-port measurements of the scattering parameters were performed through a vector network analyser (VNA) R&S® ZVA 50; each resonator was connected to a port of the VNA by using an MF141 coaxial cable and an SMA connector.

Measurements were performed by setting the R&S® ZVA 50 in order to normalise the scattering parameters to a 50 Ω impedance at both ports. A comparison between numerical and experimental

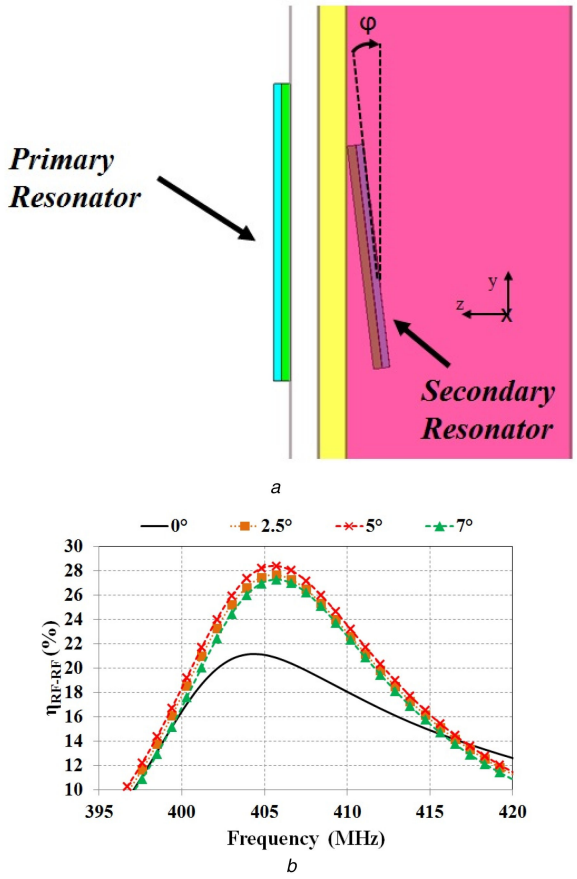

Fig. 6 *Performance calculated by full-wave simulations in the case of small rotations of the implanted resonator in the yz plane*

results is reported in Fig. 9, an overall good agreement can be observed.

The values measured at 403 MHz for the *S*-parameters are: $|S_{11}| = -11.96$ dB, $|S_{21}| = -6.87$ dB, and $|S_{22}| = -8.84$ dB.

Fig. 9*d* shows the comparison between the power transfer efficiency corresponding to measured data and the one obtained through simulations. From measurements, the maximum of η_{RF-RF} is centred at 403 MHz and it is equal to 20.54%.

5 Discussion on results: feasibility of using the WREL for recharging an IPG for DBS

In this section, the feasibility of using the proposed WREL for recharging the battery of an IPG for DBS is discussed.

The battery that is commonly adopted in modern rechargeable IPGs is a lithium-ion (Li-ion) battery with a capacity in the range of 500 µAh–325 mAh [28] and a voltage in the range of 3.7–4.1 V.

A possible system configuration of the wireless power charger is illustrated in Fig. 1; it consists of three main blocks: (i) the 50 Ω matched power source operating at 403 MHz, (ii) the wireless energy link, and (iii) the battery charger.

The role of the power source is to provide the input power P_G to the WPT link; it could be implemented by using a 50 Ω matched Class-D type RF generator [29].

As for the battery charger block, it consists of a rectifier that converts the 403 MHz signal received by the WPT link to a DC signal, and a DC/DC converter that works as a bridge between the battery and the rectifier. This latter block is crucial in battery charging applications; in fact, it converts the AC signal received by the WPT link into a DC signal satisfying the battery requirements. Referring to Fig. 1, the efficiency of the cascade of the WPT link and the battery charger is given by

$$\eta = \frac{P_{BATT}}{P_G} = \left(\frac{P_{BATT}}{P_{RX}}\right) \times \left(\frac{P_{RX}}{P_G}\right) = \eta_{CHG} \times \eta_{RF-RF} \qquad (2)$$

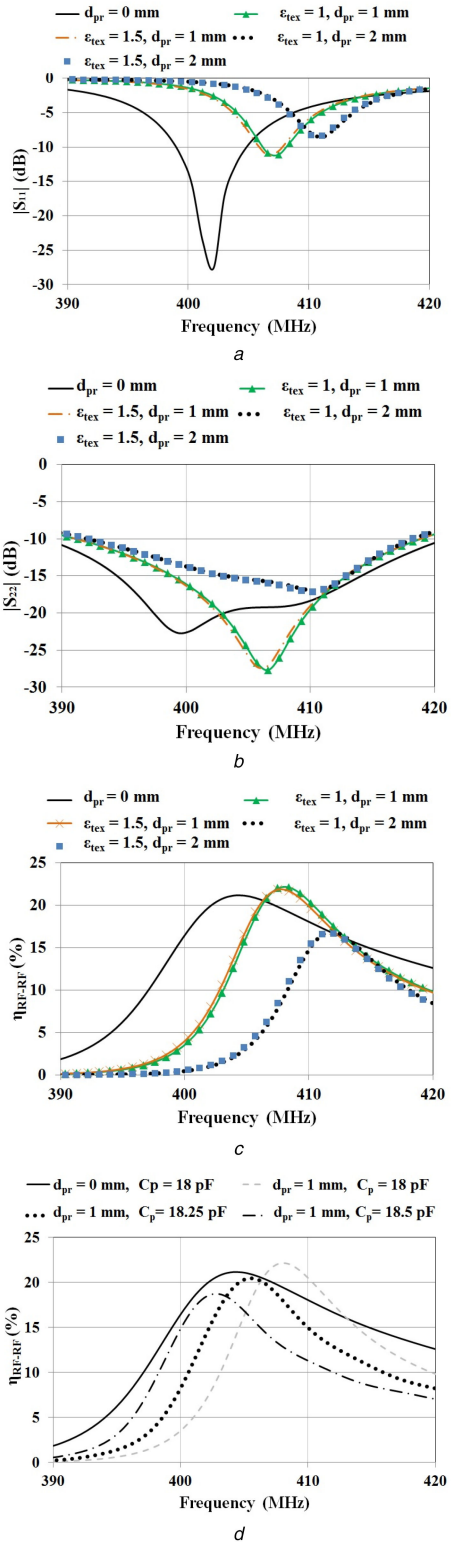

Fig. 7 *Primary resonator not in direct contact with the skin*
(a), ***(b)*** S_{11} and S_{22} scattering parameters calculated by varying the distance of the primary resonators from the skin layer, ***(c)*** Efficiency calculated by varying the distance of the primary resonators from the skin layer, ***(d)*** Efficiency calculated for $d_{pr} = 1$ mm and $\varepsilon_{tex} = 1$ for different values of the loading lumped capacitor

With regard to Li-ion batteries, the battery charger can be implemented by using a full-bridge rectifier and a DC/DC boost converter; the typical values that can be obtained for η_{CHG} are in the range of (70–90)% (for instance, a value of 90% has been assumed in [30], while a value of 77% has been obtained in [31]).

In order to evaluate the performance of the WPT link when it is connected to the battery charger, the battery charger can be modelled as a resistive load R_L [30], whose value can be optimised

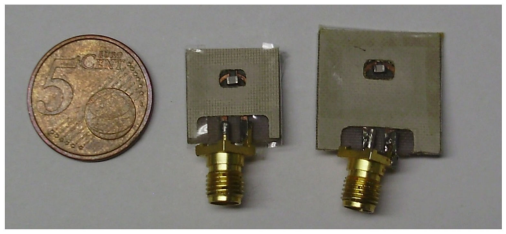

a

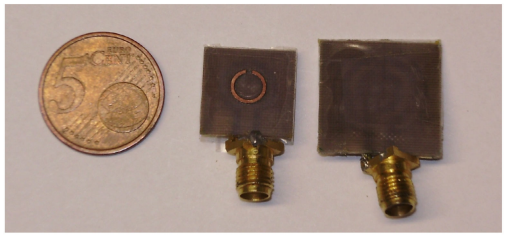

b

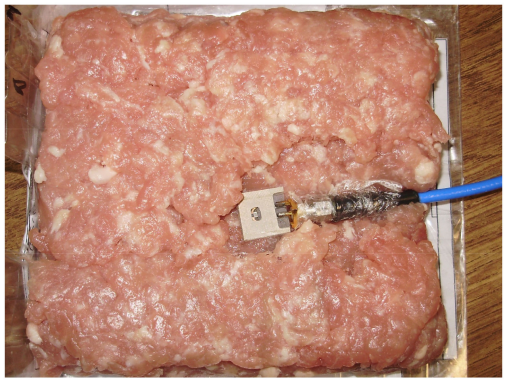

c

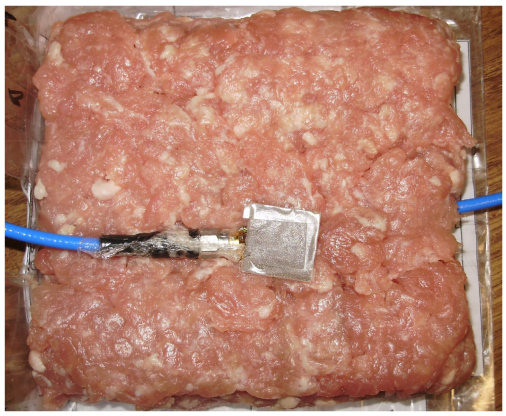

d

Fig. 8 *Photographs of the prototypes and experimental set-up for evaluating the performance of the proposed inductive link*
(a), ***(b)*** Front (on the left) and back view (on the right) of the two prototypes, ***(c)***, ***(d)*** Placement of the secondary resonator inside minced pork (on the left) and set-up adopted for measuring the scattering parameters: the primary and the secondary resonators are separated by a 5 mm thick layer of minced pork

for maximising η_{RF-RF}. In fact, according to the discussion developed in [30] and the experimental results reported in [31], the use of the DC/DC boost converter allows obtaining a value of η_{CHG} that is nearly constant over a wide range of values of the impedance seen at the input and at the output port of the battery charger [30, 31].

Accordingly, measurements were performed by varying the reference impedance of the port of the R&S® ZVA 50 VNA where was connected the secondary resonator, this being equivalent to evaluating the performance of the link for different values of R_L. While, the reference impedance at the port where was connected the primary resonator was kept constant and equal to 50 Ω (this

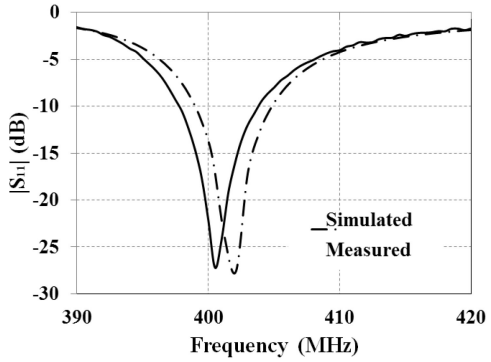

a

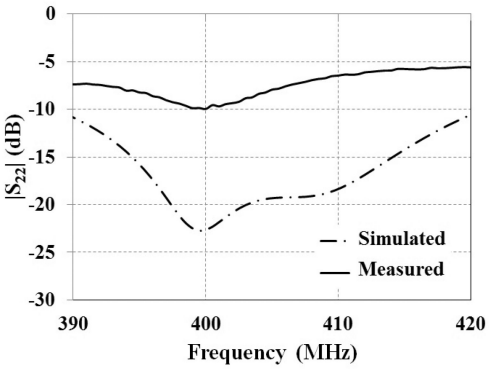

b

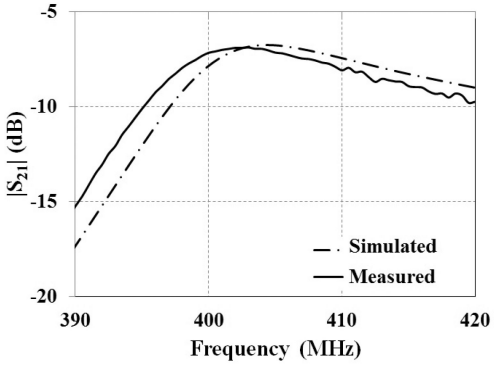

c

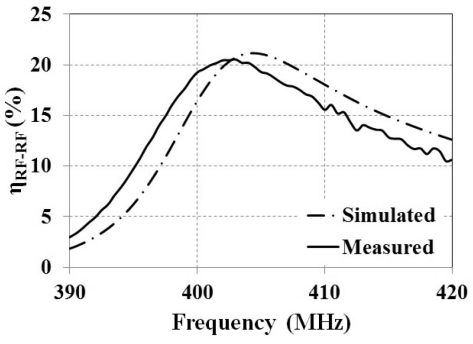

d

Fig. 9 *Comparison between numerical and experimental data obtained by using a normalisation impedance of 50 Ω at both ports obtained for*
(a)–(c) Generalised *S*-parameters, ***(d)*** RF-to-RF power transfer efficiency

being equivalent in considering $R_G = 50\ \Omega$). From experimental data, at 403 MHz, the best result for the $|S_{21}|$ was obtained for $R_L = 24\ \Omega$.

The generalised scattering parameters corresponding to the use of a reference impedance $R_G = 50\ \Omega$ at port 1 and a reference impedance $R_L = 24\ \Omega$ at port 2 are shown in Fig. 10 and are compared with the numerical data obtained by using the same reference impedances.

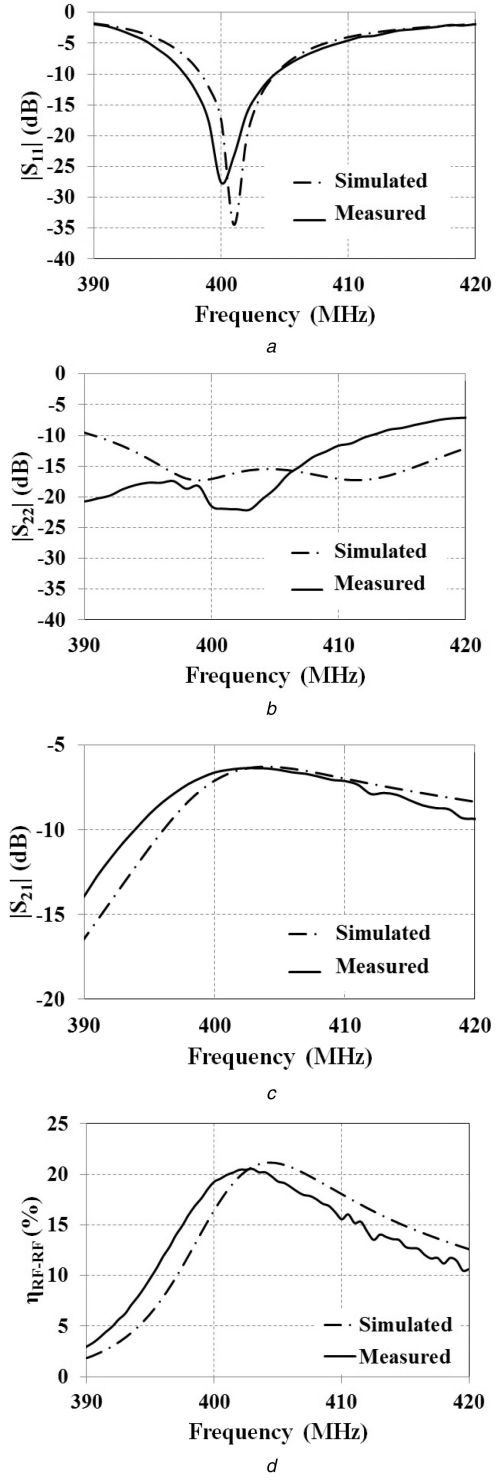

Fig. 10 *Comparison between numerical and experimental data obtained by using a normalisation impedance of 50 Ω at port 1 and a normalisation impedance of 24 Ω at port 2*
(a)–(c) Generalised *S*-parameters, ***(d)*** RF-to-RF power transfer efficiency

As it can be seen, an overall good agreement was obtained between numerical and measured data. From measurements, at 403 MHz, the η_{RF-RF} is equal to 23.17%, while from full-wave simulations, it is equal to 23.44%.

5.1 Compliance with safety regulations

The possibility of using the proposed WPT link for recharging a Li-ion battery in compliance with safety regulations has been investigated by using the simulator CST Microwave Studio.

In the frequency range of interest, safety guidelines on exposure to EM fields provide restrictions in terms of the specific absorption rate (SAR) [32–35]. Current guidelines impose limits on the peak SAR averaged on a reference mass of tissue, typically 1 or 10 g [32–35] (i.e. the peak spatial-averaged SAR). For head and trunk areas, according to the Federal Communications Commission (FCC) guidelines, the exposure limit is 1.6 W/kg for the peak 1 g average SAR, this limit is definitely more stringent than the one imposed by the International Commission on Non-Ionizing Radiation Protection (ICNIRP) guidelines which is 2 W/kg for the 10 g average SAR.

The simulator CST allows the calculation of both the 1 and the 10 g average SAR according to different standards, the results reported in the following part of this section have been calculated by using the IEEE Std C95.3-2002 [34]. The spatial-averaged SAR has been calculated by varying the value of the power provided to the primary resonator, P_G, in the range of (1–50) mW; the obtained results are summarised in Fig. 11. The spatial-averaged SAR calculated as function of P_G is given in Figs. 11*a* and *b*; the red and blue continuous lines are the 1 and the 10 g average SAR, respectively; while, the dashed lines have been used to indicate the limit imposed on the 1 g average SAR by the FCC (red dashed line) and the one imposed on the 10 g average SAR by the ICNIRP (blue dashed line).

In order to satisfy the FCC guidelines, a value of $P_G < 4.8$ mW has to be used; while the value of P_G which allows to satisfy the ICNIRP guidelines is 38 mW (i.e. $P_G < 39$ mW).

Fig. 11*c* shows the simulated 1 g average SAR distribution calculated by means of full-wave simulations at 403 MHz for $P_G =$ 4.7 mW.

5.2 Recharging of an Li-ion battery

The time necessary for recharging a battery with a capacity C can be calculated according to the following formula:

$$T_{charge} = \frac{C}{I_{charge}} \tag{3}$$

where I_{charge} is the charging current which can be calculated as the ratio between the power provided to the battery and the charging voltage

$$I_{charge} = \frac{P_{BATT}}{V_{charge}} \tag{4}$$

In order to lengthen the life time of an Li-ion battery, a full discharge should be avoided. A good practice is to recharge the battery when its charge is 20% below the maximum level. Accordingly, by using (3) and (4), the time necessary for recharging the battery is given by

$$T_{charge} = 0.2 \times \frac{C}{P_{BATT}/V_{charge}} \tag{5}$$

Referring to Fig. 1 and by using (2), for the proposed wireless battery charger P_{BATT} is given by

$$P_{BATT} = \eta_{CHG} \times \eta_{RF-RF} \times P_G \tag{6}$$

where η_{RF-RF} is the efficiency of the WPT link while η_{CHG} is the efficiency of the battery charger. Equations (5) and (6) can be used for determining the maximum capacity C_{max} of an Li-ion battery that can be charged by using the proposed WPT link with a reasonable charging time:

$$C_{max} = \eta_{CHG} \times \eta_{RF-RF} \times P_G \times \frac{1}{V_{charge}} \times \frac{T_{charge}}{0.2} \tag{7}$$

The values obtained by using (7) are reported in Figs. 11*a* and *b*; calculations have been performed by using for η_{RF-RF} the value of 23.17% obtained by measurements. The value adopted for V_{charge} is 4.1 V, which is the maximum value assumed by the charging

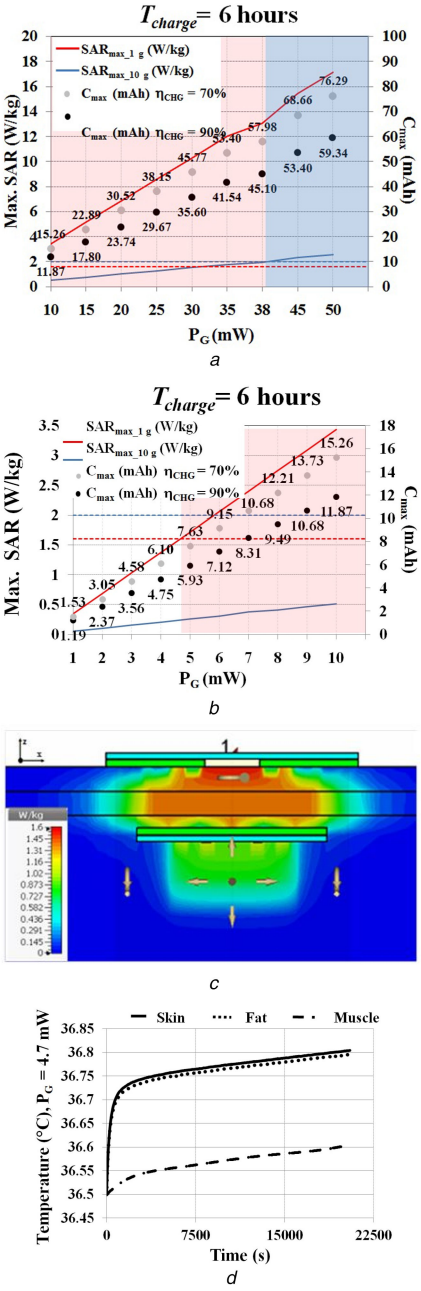

Fig. 11 *Results obtained for the 1 and the 10 g average SAR and for the values of the capacity of a Li-ion battery that can be recharged in a recharging time (T_{charge}) of 6 h*

(a), ***(b)*** Results obtained for the 1 g (red continuous line) and the 10 g average SAR (blue continuous line). The values of the capacity of an Li-ion battery that can be recharged in a recharging time of 6 h are also reported (dots). The black dots refer to the case of a battery charger with an efficiency η_{CHG} equal to 70%; while the grey dots refer to the case a battery charger with an efficiency η_{CHG} equal to 90%, ***(c)*** Simulated 1 g average SAR distribution at 403 MHz when P_G was equal to 4.7 mW, ***(d)*** Temperature rise behaviour obtained for P_G equal to 4.7 mW

voltage of a typical Li-ion battery. As per T_{charge}, a value of 6 h has been considered; in fact, considering the intended application (i.e. the recharge of a medical device), a reasonable value for the recharging time could be a value <8 h.

As for η_{CHG}, both the case of η_{CHG} = 70% (black dots) and the case of η_{CHG} = 90% (grey dots) have been considered.

As it can be seen, the maximum value of the capacity of an Li-ion battery that can recharged in a charging time of 6 h is between 5.6 (for η_{CHG} = 70%) and 7.2 mAh (for η_{CHG} = 90%), when the power provided to the transmitting resonator is set in compliance with the FCC guidelines (i.e. P_G = 4.7 mW).

Finally, the thermal solver of the CST simulator was used in order to calculate the temperature rise (ΔT) in human tissues. The achieved results are given in Fig. 11*d*; for each of the three simulated tissues (i.e. skin, fat, and muscle), the figure shows the temperature behaviour in the point where the maximum (ΔT) was observed. As it can be seen, a maximum of 0.3°C was achieved in the skin tissues.

According to the results reported in this section, it is possible to conclude that the proposed link is suitable to be used for recharging a medical device implanted at a few millimetres of depth and having a battery with a capacity of the order of a few milliampere hour.

6 Conclusion

In this paper, the feasibility of using the MedRadio band for implementing a wireless charger for medical devices implanted in the chest was investigated.

Experimental and numerical data referring to a WREL operating at 403 MHz were reported showing that a power transfer efficiency of ~23% can be obtained. Although this value is definitely lower than the ones reported in the literature for links operating at some hundreds of kilohertz, it has been demonstrated that the achieved value of the efficiency is sufficient to recharge a medical device with an implantation depth of few millimetres and using an Li-ion battery with a capacity of the order of a few milliampere hour.

In more detail, the value of 23% that has been obtained for the efficiency allows the recharging of an Li-ion battery implanted at a depth of 5 mm and having a capacity up to 7 mAh in 6 h and in compliance with both the limit imposed by the FCC guidelines on the 1 g average SAR and the one imposed by the ICNIR guidelines on the 10 g average SAR.

7 Acknowledgments

This work was supported by 'Fondo di Sviluppo e Coesione 2007–2013 – APQ Ricerca Regione Puglia 'Programma regionale a sostegno della specializzazione intelligente e della sostenibilità sociale ed ambientale – FutureInResearch'.

8 References

[1] Pluta, R.M., Perazza, G.D., Golub, R.M.: 'Deep brain stimulation', *JAMA*, 2011, **305**, (7), p. 732

[2] Lee, H.M., Park, H., Ghovanloo, M.: 'A power-efficient wireless system with adaptive supply control for deep brain stimulation', *IEEE J. Solid-State Circuits*, 2013, **48**, (9), pp. 2203–2216

[3] 'Boston scientific – Vercise™ deep brain stimulation system'. Available at http://www.vercise.com/vercise-and-guide-dbs-systems/vercise-dbs/, accessed 24 June 2016

[4] 'Medtronic – activa RC neurostimulator'. Available at http://professional.medtronic.com/pt/neuro/dbs-md/prod/activa-rc/index.htm#.V2zziaKDugM, accessed 24 June 2016

[5] Monti, G., Corchia, L., Tarricone, L.: 'ISM band rectenna using a ring loaded monopole', *Prog. Electromagn. Res. C*, 2012, **33**, pp. 1–15

[6] Monti, G., Corchia, L., Tarricone, L.: 'A wearable wireless energy link'. 2015 European Microwave Conference (EuMC), Paris, 2015, pp. 143–146

[7] Monti, G., Congedo, F.: 'UHF rectenna using a bowtie antenna', *Prog. Electromagn. Res. C*, 2011, **26**, pp. 181–192

[8] Jow, U.M., Ghovanloo, M.: 'Design and optimization of printed spiral coils for efficient inductive power transmission'. IEEE Int. Conf. on Electronics, Circuits and Systems (ICECS), Marrakech, Morocco, December 2007, pp. 70–73

[9] Campi, T., Cruciani, S., Palandrani, , *et al.*: 'Wireless power transfer charging system for AIMDs and pacemakers', *IEEE Trans. Microw. Theory Techn.*, 2016, **64**, (2), pp. 633–642

[10] Khripkov, A., Hong, W., Pavlov, K.: 'Integrated resonant structure for simultaneous wireless power transfer and data telemetry', *IEEE Antennas Wirel. Propag. Lett.*, 2012, **11**, pp. 1659–1662

[11] Jegadeesan, R., Guo, Y.X., Xue, R.F., *et al.*: 'An efficient wireless power link for neural implant'. IEEE Int. Symp. on Radio-Frequency Integration Technology (RFIT), Singapore, November 2012, pp. 122–124

[12] Wu, W., Fang, Q.: 'Design and simulation of printed spiral coil used in wireless power transmission systems for implant medical devices'. Int. Conf. of the IEEE Engineering in Medicine and Biology Society, Boston, MA, 2011, pp. 4018–4021

[13] Monti, G., Arcuti, P., Tarricone, L.: 'Resonant inductive link for remote powering of pacemakers', *IEEE Trans. Microw. Theory Tech.*, 2015, **63**, (11), pp. 3814–3822

[14] 'FCC (Federal Communications Commission) – medical device radiocommunications service'. Available at https://www.fcc.gov/general/medical-device-radiocommunications-service-medradio, accessed 24 June 2016
[15] Monti, G., De Paolis, M.V., Tarricone, L.: 'Wireless power transfer link for rechargeable deep brain stimulators'. IEEE 15th Mediterranean Microwave Symp. (MMS), Lecce, Italy, 2015, pp. 1–4
[16] Monti, G., De Paolis, M.V., Tarricone, L.: 'Wireless energy link for deep brain stimulation'. 2015 European Microwave Conf. (EuMC), Paris, 2015, pp. 64–67
[17] Kurs, A., Karalis, A., Moffatt, R., *et al.*: 'Wireless power transfer via strongly coupled magnetic resonances', *Science*, 2007, **317**, pp. 83–86
[18] Monti, G., Tarricone, L., Dionigi, M., *et al.*: 'Magnetically coupled resonant wireless power transmission: an artificial transmission line approach'. European Microwave Conf. (EuMC), Amsterdam, Netherlands, 2012, pp. 233–236
[19] Dionigi, M., Costanzo, A., Mastri, F., *et al.*: 'Recent advances on magnetic resonant wireless power transfer', in Agbinya, J.I. (Ed.): '*Wireless power transfer*' (River Publishers, Gistrup, Denmark, 2016, 2nd edn.), pp. 217–270
[20] Collin, R.E.: '*Foundations for microwave engineering*' (Wiley-IEEE Press, Hoboken, New Jersey, 2001, 2nd edn.)
[21] Inagaki, N.: 'Theory of image impedance matching for inductively coupled power transfer systems', *IEEE Trans. Microw. Theory Tech.*, 2014, **62**, (4), pp. 901–908
[22] Das, R., Yoo, H.: 'Biotelemetry and wireless powering for leadless pacemaker systems', *IEEE Microw. Wirel. Compon. Lett.*, 2015, **25**, (4), pp. 262–264
[23] Kim, S., Ho, J.S., Chen, L.Y., *et al.*: 'Wireless power transfer to a cardiac implant', *Appl. Phys. Lett.*, 2012, **101**, pp. 073701-1–073701-4
[24] 'IT'IS Foundation – database at a glance'. Available at http://www.itis.ethz.ch/itis-for-health/tissue-properties/database/, accessed 24 June 2016
[25] Clarys, J.P., Marfell-Jones, M.: 'Body composition: part 1 physical and structural distribution of human skin', in Reilly, T. (Ed.): '*Musculoskeletal disorders in health-related occupations*' (IOS Press, Amsterdam, 2002), pp. 143–147
[26] Horejsi, R., Möller, R., Pieber, , *et al.*: 'Differences of subcutaneous adipose tissue topography between type-2 diabetic men and healthy controls', *Exp. Biol. Med. (Maywood)*, 2002, **227**, (9), pp. 794–798
[27] Monti, G., Tarricone, L., Trane, C.: 'Experimental characterization of a 434 MHz wireless energy link for medical applications', *Prog. Electromagn. Res. C*, 2012, **30**, pp. 53–64
[28] 'EaglePicher technologies – Li-ion family'. Available at http://www.eaglepicher.com/li-ion-family, accessed 24 June 2016
[29] Fu, M., Zhang, T., Zhu, X., *et al.*: 'A 13.56 MHz wireless power transfer system without impedance matching networks'. Wireless Power Transfer (WPT), Perugia, Italy, May 2013, pp. 222–225
[30] Campi, T., Cruciani, S., De Santis, V., *et al.*: 'EMF safety and thermal aspects in a pacemaker equipped with a wireless power transfer system working at low frequency', *IEEE Trans. Microw. Theory Tech.*, 2016, **64**, (2), pp. 375–382
[31] Fu, M., Ma, C., Zhu, X.: 'A cascaded boost–buck converter for high-efficiency wireless power transfer systems', *IEEE Trans. Ind. Informat.*, 2014, **10**, (3), pp. 1972–1980
[32] IEEE Standard C95.1, 2005: 'IEEE standard for safety levels with respect to human exposure to radiofrequency electromagnetic fields, 3 kHz to 300 GHz', 2005
[33] Guideline, ICNIRP: 'Guidelines for limiting exposure to time-varying electric, magnetic, and electromagnetic fields (up to 300 GHz)', *Health Phys.*, 1998, **74**, (4), pp. 494–522
[34] IEEE Std C95.3-2002: 'IEEE recommended practice for measurements and computations of radio frequency electromagnetic fields with respect to human exposure to such fields, 100 kHz–300 GHz' (revision of IEEE Std C95.3-1991), 2002
[35] Federal Communications Commission Office of Engineering & Technology OET Bulletin 65: 'Evaluating compliance with FCC guidelines for human exposure to radiofrequency electromagnetic fields', Edition 97-01, August 1997